

## Journal Pre-proofs

On-line Optimization of Four-Zone Simulated Moving Bed Chromatography using an Equilibrium-Dispersion Model: I. Simulation Study

Ju Weon Lee, Achim Kienle, Andreas Seidel-Morgenstern

PII: S0009-2509(20)30342-0  
DOI: <https://doi.org/10.1016/j.ces.2020.115810>  
Reference: CES 115810

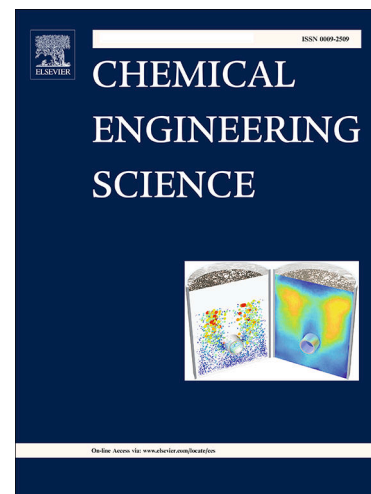
To appear in: *Chemical Engineering Science*

Received Date: 12 November 2019  
Revised Date: 8 April 2020  
Accepted Date: 14 May 2020

Please cite this article as: J. Weon Lee, A. Kienle, A. Seidel-Morgenstern, On-line Optimization of Four-Zone Simulated Moving Bed Chromatography using an Equilibrium-Dispersion Model: I. Simulation Study, *Chemical Engineering Science* (2020), doi: <https://doi.org/10.1016/j.ces.2020.115810>

This is a PDF file of an article that has undergone enhancements after acceptance, such as the addition of a cover page and metadata, and formatting for readability, but it is not yet the definitive version of record. This version will undergo additional copyediting, typesetting and review before it is published in its final form, but we are providing this version to give early visibility of the article. Please note that, during the production process, errors may be discovered which could affect the content, and all legal disclaimers that apply to the journal pertain.

© 2020 Published by Elsevier Ltd.



# On-line Optimization of Four-Zone Simulated Moving Bed Chromatography using an Equilibrium-Dispersion Model:

## I. Simulation Study

Ju Weon Lee<sup>1,\*</sup>, Achim Kienle<sup>1,2</sup>, and Andreas Seidel-Morgenstern<sup>1,3</sup>

<sup>1</sup> Max-Planck-Institute for Dynamics of Complex Technical Systems  
Sandtorstr. 1, 39106 Magdeburg, Germany

<sup>2</sup> Institute of Automation Technology, Otto von Guericke University  
Universitätsplatz 2, 39106 Magdeburg, Germany

<sup>3</sup> Institute of Process Engineering, Otto von Guericke University  
Universitätsplatz 2, 39106 Magdeburg, Germany

\*: Corresponding Author

Tel: +49 391 6110392

Fax: +49 391 6110521

Email: [lee@mpi-magdeburg.mpg.de](mailto:lee@mpi-magdeburg.mpg.de)

**Abstract**

Simulated moving bed (SMB) chromatographic processes have been successfully applied to petrochemical, pharmaceutical, and fine chemical industries to separate the target products with high purity and yield since it was introduced in 1960s. Conventional four-zone SMB chromatography and its advanced variants are nowadays the most promising continuous processes for the separation of chiral active pharmaceutical ingredients (APIs). However, the design and optimization of SMB processes is still challenging issues due to their structural complexity and operational sensitivity. In this work, the equilibrium-dispersion model with nonlinear adsorption isotherms was applied for model based on-line optimization. The proposed optimization technique estimates the process states including the isotherm and kinetic parameters. The operating conditions are dynamically optimized 'switch-by-switch' in order to separate binary mixtures up to 99% product purity.

Keywords: On-line optimization, Simulated moving bed chromatography, Equilibrium-dispersion model, Nonlinear isotherms, Mixing cell with active counteraction scheme, Bicalutamide enantiomers

## 1. Introduction

The simulated moving bed (SMB) process was introduced in 1960s [1]. Since then various operational and structural configurations were developed to enhance process performance [2]. The conventional four-zone SMB process capable to perform binary or pseudo-binary separations exploits a closed ring of several packed-bed columns. This ring is divided into four zones by two inlets (the feed and the desorbent streams) and two outlets (the extract and the raffinate streams) as shown in Figure 1. Either, the positions of four inlet and outlet ports are shifted in the direction of the liquid phase flow, or the columns are shifted to the opposite direction to simulate a counter-current flow of the solid phase. A feed mixture continuously enters the process through the feed port. The desorbent, which has typically the same solvent composition as the feed, continuously enters the process through the desorbent port. The mixture components are separated in the packed-bed columns and collected at two outlets, the less-retained component at the raffinate port and the more-retained component at the extract port. Because of the periodic repetition of the ports or the column switching, the SMB process does not reach a steady-state but a cyclic steady-state (CSS) after a certain number of switches.

The SMB process is conventionally designed in several steps as shown in Figure 2 (Conventional Design Steps). The first step is a feasibility test. Several mobile and stationary phases are screened to find suitable combinations by examining the basic properties, e.g. solubility, column efficiency, and separation selectivity. In the second step, a mechanistic process model that can represent the chosen separation mechanism is applied, and the essential parameters, e.g. isotherm and kinetic parameters, are measured on an analytical scale. Using the chosen process model, a suitable process configuration is selected and the optimal operating conditions are determined. The latter are the liquid flow rates in the zones and the switching time. Generally, one condition, e.g. the feed flow-rate or the port switching interval, is fixed due to feed requirements or operational constraints, so that the remaining operating conditions need to be calculated. Initial guesses can be provided by short-cut methods such as the triangle theory [3] and the standing-wave method [4]. They can be further refined by simulation or offline optimization [5, 6]. At last, the determined process conditions are experimentally validated. Due to plant model mismatch, iterative refinement from the second to the

last step may be required until the process performance satisfies the given design criteria, e.g. purity and yield of the target component. This conventional design campaign requires relatively long development time and huge investment resources due to the iterative approach. Alternatively, model based optimization in combination with parameter estimation can be directly applied to the pilot-scale plant to determine the operating conditions on-line in relatively short time and thereby reduce the design effort significantly as illustrated in Figure 2 (Proposed Design Steps). A necessary prerequisite for this approach is the availability of fast optimization, which can be completed within one switching interval of the SMB process.

The approach described in this paper can be viewed as a limiting case of more general model predictive control concepts, which have been developed in the past for SMB processes. In model predictive control, repetitive on-line optimization is applied to calculate a sequence of optimal control moves over a finite time horizon to drive the process to the desired target. The first move is implemented and the strategy is repeated after readjustment of the process model with updated on-line measurement information from the process. This control strategy is very powerful but also computationally expensive if a rigorous process model is applied. The computational effort can be reduced applying advanced numerical methods [7, 8], the use of linearized models which are adapted on-line to the process conditions [9], cycle to cycle [10] and multirate control strategies to exploit fast measurement information [11]. A detailed literature review on control and, in particular, model predictive control of SMB processes with many additional references can be found in [12]. An updated review is in press [13].

In the present paper a new approach for the online optimization of SMB processes is presented. It is simple, robust and fast. *Simplicity* follows from the fact that only optimization of final cyclic steady states is considered. Transient towards cyclic steady state is not optimized in contrast to the previous work on model predictive control mentioned above. *Robustness* follows from the fact that a rigorous nonlinear process models used, i.e. the well-established equilibrium-dispersion model with nonlinear isotherms. Linearization is not applied. The algorithm is *fast* because a new solution algorithm is applied: The mixing cell with active counteraction (MC-AC) scheme [14] was used to

accelerate the computation for updating the process model parameters and to search the optimized operating conditions in every control cycle corresponding to one port switching interval. Further, an additional concentration measurement in the recycle was considered, to allow tighter control. It is shown that the new algorithm together with the additional measurement information performs very well also in comparison to previous approaches, especially for high feed concentrations in the nonlinear range of the adsorption isotherm considered in this paper. Application is demonstrated for the separation of bicalutamide racemates. Bicalutamide is an active pharmaceutical ingredient (API) against prostate cancer. It is available on the market (Casodex®, AstraZeneca) as a racemic mixture. The (R)-form enantiomer is the active eutomer. Thus, the other undesired (S)-form enantiomer should be separated for further racemization to increase productivity [15].

## 2. Modeling of SMB Process

The mathematical process model consists of the material balances in the chromatographic columns and at the inlet and outlet ports in Figure 1. The latter depends on the mode of operation.

### 2.1. Column models

The chromatographic columns are described by a material balance based model with axial dispersion in the liquid phase and a linear driving for the mass transfer between the liquid and the solid phase, according to

$$v_L \frac{\partial c_i}{\partial z} + \varepsilon \frac{\partial c_i}{\partial t} + (1 - \varepsilon) \frac{\partial q_i}{\partial t} = \varepsilon D_L \frac{\partial^2 c_i}{\partial z^2}, \quad \forall i \in \mathbf{N}_S \quad (1)$$

$$\frac{\partial q_i}{\partial t} = k_{eff,i} (q_i^* - q_i) \quad (2)$$

where  $v_L$  is the linear velocity of the mobile phase ( $= \varepsilon u_L$ ,  $u_L$  is the interstitial velocity of the mobile phase),  $\varepsilon$  is the inter-particle void fraction of the column,  $D_L$  is the longitudinal dispersion coefficient,  $\mathbf{N}_S$  is the set of solutes in the feed mixture,  $k_{eff}$  is the mass transfer coefficient,  $c$  is the concentration in the liquid phase,  $q^*$  is the equilibrium concentration of solute  $i$  on the solid film,  $q$  is the concentration in the solid phase, and the subscript  $i$  denotes the solute  $i$  in the solute set,  $\mathbf{N}_S$ .

In many cases of adsorption chromatography, the Langmuir isotherm model can be used to describe the adsorption equilibrium,

$$q_i^* = q_{Max1} \frac{K_i c_i}{1 + \sum_{\forall l \in \mathbf{N}_S} K_l c_l} \quad (3)$$

where  $q_{Max}$  is the maximum adsorption capacity and  $K_i$  is the equilibrium constant of solute  $i$ . To satisfy thermodynamic consistency,  $q_{Max}$  should be the same for all components. For dilute concentrations, Eq. (3) can be simplified to the linear isotherms, and the Henry's constants are equivalent to  $q_{Max} K_i$ . In enantioselective separations with chiral chromatographic columns, it is commonly assumed that the adsorbents have two active sites; one has chiral recognition properties, but the other has not. Therefore, the bi-Langmuir (also called dual-site Langmuir) isotherm model is commonly used to describe equilibrium for chiral separation cases.

$$q_i^* = q_{1,Max} \frac{K_1 c_i}{1 + K_1 \sum_{\forall l \in \mathbf{N}_S} c_l} + q_{2,Max} \frac{K_{2,i} c_i}{1 + \sum_{\forall l \in \mathbf{N}_S} K_{2,l} c_l} \quad (4)$$

where the subscripts 1 and 2 denote the achiral and chiral active sites respectively. For dilute concentrations, the Henry's constants are equivalent to  $q_{1,Max} K_1 + q_{2,Max} K_{2,i}$ . In this paper, the above process model, Eqs. (1) and (2), and the bi-Langmuir isotherm model were applied to simulate the SMB process using a commercial simulator. Detailed information with parameters of bicalutamides [15] is in Table 1.

For parameter estimation and optimization purposes, a simpler equilibrium-dispersion model was used in this paper according to

$$v_L \frac{\partial c_i}{\partial z} + \varepsilon \frac{\partial c_i}{\partial t} + (1 - \varepsilon) \frac{\partial q_i}{\partial t} = \varepsilon D_{a,i} \frac{\partial^2 c_i}{\partial z^2}, \quad \forall i \in \mathbf{N}_S \quad (5)$$

where  $D_{a,i}$  is the apparent dispersion coefficient of solute  $i$ , which lumps together the band broadening effects due to axial dispersion and finite mass transfer resistance. In this model the mass transfer resistance between the liquid and the solid phases is neglected and promptly established thermodynamic equilibrium is assumed ( $q_i = q_i^*$ ). Hence, the solid phase concentrations,  $q_i$  follow directly the liquid phase concentrations according to the adsorption isotherms (Eqs. (3) or (4)).

To optimize the SMB process switch-by-switch, parameter estimation and process optimization must be completed in one port switching interval, which is typically in the range of a few

minutes in this work. To achieve a new efficient numerical approach for the simulation of the equilibrium-dispersion model, a recently developed rapid numerical method, MC-AC scheme was applied. It is based on exploiting a discretized mixing cell model and introduces artificial negative dispersion to compensate for numerical dispersion, which occurs if the number of mixing cells is low. With this scheme, steep concentration profiles can be quickly and accurately resolved with a rather small number of mixing cells. Details are given in reference [14].

## 2.2. Balances of the inlet and outlet ports and advanced SMB operating modes

In the standard operation of four-zone SMB process, all flow-rates are constant during a port switching interval. This means that the mixture feeding and product collection can be done without flow intermittence. At the given operating conditions (zone flow-rates and port switching interval), the zone inlet conditions, which are the boundary conditions for the PDE system representing the material balances in each zone, can be determined as,

$$Q_{L,Z1}^{Std} = Q_{L,Z4}^{Std} + Q_{L,Dsrb}^{Std}, \quad c_{i,Z1In}^{Std} = \frac{c_{i,Z4Out}^{Std} Q_{L,Z4}^{Std} + c_{i,Dsrb}^{Std} Q_{L,Dsrb}^{Std}}{Q_{L,Z4}^{Std} + Q_{L,Dsrb}^{Std}} \quad (6-1)$$

$$Q_{L,Z2}^{Std} = Q_{L,Z1}^{Std} - Q_{L,Extr}^{Std}, \quad c_{i,Z2In}^{Std} = c_{i,Extr}^{Std} = c_{i,Z1Out}^{Std} \quad (6-2)$$

$$Q_{L,Z3}^{Std} = Q_{L,Z2}^{Std} + Q_{L,Feed}^{Std}, \quad c_{i,Z3In}^{Std} = \frac{c_{i,Z2Out}^{Std} Q_{L,Z2}^{Std} + c_{i,Feed}^{Std} Q_{L,Feed}^{Std}}{Q_{L,Z2}^{Std} + Q_{L,Feed}^{Std}} \quad (6-3)$$

$$Q_{L,Z4}^{Std} = Q_{L,Z3}^{Std} - Q_{L,Raff}^{Std}, \quad c_{i,Z4In}^{Std} = c_{i,Raff}^{Std} = c_{i,Z1Out}^{Std} \quad (6-4)$$

where  $Q_L$  is the volumetric flow-rate of the mobile phase, the superscript, *Std* denotes the standard operation, the subscripts, *Dsrb*, *Extr*, *Feed*, and *Raff* respectively denote the desorbent, extract, feed, and raffinate (see Figure 1), and the subscripts,  $Z_n$ ,  $Z_nIn$ , and  $Z_nOut$  denote the  $n^{\text{th}}$  zone and its inlet and outlet, respectively.

Based on this standard SMB operation, many more advanced operational strategies were introduced to improve the process performances [2]. In this work, two advanced operating modes that can be easily implemented by manipulating the zone flow-rates without changing feed concentrations or breaking the synchronous port switching were applied.

The first one is the outlet stream swing (OSS) operation [16]. In this operation, the feed and desorbent flow-rates are constant, but the two outlet streams are intermittently closed in every period of the port switching interval. To meet the overall material balance, one outlet flow is the summation of two inlet flows while the other outlet flow is zero. Assuming that the zones 1 and 4 are successful in regenerating adsorbent and desorbent, i.e. there is no product contamination through the desorbent port, the extract stream is closed at the beginning of the port switching interval, because impurities in the extract elute at the beginning of the interval. On the reverse, the raffinate stream is closed at the end of the port switching interval, because impurities in the raffinate elute at the end of the interval, cf. Appendix A.

The changes of product flows of the OSS operation can be divided into three steps as below,

Step 1: Extract stream off

$$Q_{L,Z1}^{OSS1} = Q_{L,Z2}^{OSS1} = Q_{L,Z1}^{Std} \quad (7-1)$$

$$Q_{L,Z3}^{OSS1} = Q_{L,Z1}^{Std} + Q_{L,Feed}^{Std} \quad (7-2)$$

$$Q_{L,Z4}^{OSS1} = Q_{L,Z1}^{Std} + Q_{L,Feed}^{Std} - Q_{L,Extr}^{Std} - Q_{L,Raff}^{Std} \quad (7-3)$$

$$t_S^{OSS1} = \frac{Q_{L,Raff}^{Std}}{Q_{L,Extr}^{Std} + Q_{L,Raff}^{Std}} (1 - F_{Op}^{OSS}) t_S^{Std}, \quad 0 \leq F_{Op}^{OSS} \leq 1 \quad (7-4)$$

Step 2: Standard operation

$$Q_{L,j}^{OSS2} = Q_{L,j}^{Std}, \quad \forall j \in \{Z1, \dots, Z4\} \quad (7-5)$$

$$t_S^{OSS2} = F_{Op}^{OSS} t_S^{Std} \quad (7-6)$$

Step 3: Raffinate stream off

$$Q_{L,Z1}^{OSS3} = Q_{L,Z1}^{Std} \quad (7-7)$$

$$Q_{L,Z2}^{OSS3} = \max(0, Q_{L,Z1}^{Std} - Q_{L,Extr}^{Std} - Q_{L,Raff}^{Std}) \quad (7-8)$$

$$Q_{L,Z3}^{OSS3} = Q_{L,Z4}^{OSS3} = Q_{L,Z1}^{Std} - Q_{L,Extr}^{Std} - Q_{L,Raff}^{Std} + Q_{L,Feed}^{Std} \quad (7-9)$$

$$t_S^{OSS3} = \frac{Q_{L,Extr}^{Std}}{Q_{L,Extr}^{Std} + Q_{L,Raff}^{Std}} (1 - F_{Op}^{OSS}) t_S^{Std} \quad (7-10)$$

where  $t_S$  is the port switching interval,  $F_{Op}$  is the operation factor that determines the length of the second step, the superscript,  $OSSn$  denotes the  $n^{\text{th}}$  OSS operation step. In this work, the flow rates of the zones 1 and 4 of the OSS operation are taken as the same as these of the standard operation, so that

the extract flow-rate in the last step of the OSS operation can be greater than the flow rate of the zone 1 if the flow rate of the zone 4 ( $Q_{L,Z4}^{Std}$ ) is smaller than the feed flow-rate ( $Q_{L,Feed}^{Std}$ ) in the corresponding standard operation. This means the liquid flow direction in the zone 2 can be reversed. A reversed zone flow-rate can cause serious problems in certain configurations, in which the outlet stream flow-rates are directly controlled by the pumps. To avoid this flow reversal problem, the flow rate of the zone 2 is constrained to be greater than or equal to zero, and the feed flow-rate is correspondingly reduced, cf. Eqs. (7-8) and (7-9).

The second one is the flow-focusing (FF) operation. In this operation, all inlets and outlets are intermittently opened and closed depending on the position of the internal concentration profiles. To modulate the position of the internal concentration profiles, the liquid phase is internally circulated and all external flows are closed at the beginning and the end of the port switching interval. On the reverse, all external flows are opened during the rest of the port switching interval. Since the flows are focused in a narrower time interval than the standard operation, the external flows are increased to have the same average zone flow-rates of the corresponding standard operation. One variation of this operation concept is so called the Intermittent-SMB process [17], cf. Appendix A.

In this work, a three-step intermittent operating mode is introduced as described in the following,

Step 1: Internal circulation

$$Q_{L,Z1}^{FF1} = Q_{L,Z2}^{FF1} = Q_{L,Z3}^{FF1} = Q_{L,Z4}^{FF1} = Q_{L,Z4}^{Std} \quad (8-1)$$

$$t_S^{FF1} = F_{Pos}^{FF} (1 - F_{Op}^{FF}) t_S^{Std}, \quad 0 \leq F_{Pos}^{FF} \leq 1, \quad 0 < F_{Op}^{FF} \leq 1 \quad (8-2)$$

Step 2: Focused external flows

$$Q_{L,Z1}^{FF2} = Q_{L,Z4}^{Std} + Q_{Feed}^{Std} / F_{Op}^{FF} \quad (8-3)$$

$$Q_{L,Z2}^{FF2} = Q_{L,Z4}^{Std} + (Q_{L,Feed}^{Std} - Q_{L,Extr}^{Std}) / F_{Op}^{FF} \quad (8-4)$$

$$Q_{L,Z3}^{FF2} = Q_{L,Z4}^{Std} + (Q_{L,Feed}^{Std} - Q_{L,Extr}^{Std} + Q_{L,Feed}^{Std}) / F_{Op}^{FF} \quad (8-5)$$

$$Q_{L,Z3}^{FF2} = Q_{L,Z4}^{Std} + (Q_{L,Feed}^{Std} - Q_{L,Extr}^{Std} + Q_{L,Feed}^{Std} - Q_{L,Raff}^{Std}) / F_{Op}^{FF} \quad (8-6)$$

$$t_S^{FF2} = F_{Op}^{FF} t_S^{Std} \quad (8-7)$$

Step 3: Internal circulation

$$Q_{L,Z1}^{FF1} = Q_{L,Z2}^{FF1} = Q_{L,Z3}^{FF1} = Q_{L,Z4}^{FF1} = Q_{L,Z4}^{Std} \quad (8-8)$$

$$t_S^{FF3} = (1 - F_{Pos}^{FF})(1 - F_{Op}^{FF})t_S^{Std} \quad (8-9)$$

where  $F_{Pos}$  is the position factor of the focused external flows, the superscript  $FF$  denotes the FF operation, and  $FFn$  denotes the  $n^{\text{th}}$  FF operation step. In the first and last steps, the liquid phase is only internally circulated with the zone 4 flow-rate of the corresponding standard operation to locate the internal profiles in proper position. In the second step, the external inlet and outlet flows are focused with higher flows than the corresponding standard operation flows.

When the operation factors for the OSS and FF operations are equal to 1, these advanced SMB operating modes are the same as the standard SMB operation. In the OSS operation, the operation factor  $F_{Op}^{OSS}$  can be zero, i.e. there is no second step (that is the same as the standard SMB operation). However, the operation factor for the FF operation,  $F_{Op}^{FF}$  must be greater than zero to have the focused second step. Any standard operation can be extended to the OSS or the FF operations that has the same average zone flow-rates for one port switching interval except  $Q_{L,1}^{Std} < Q_{L,Extr}^{Std} + Q_{L,Raff}^{Std}$  for the OSS operation.

### 3. On-line Optimization Strategy

In a previous work [15], an SMB process for the separation of bicalutamide enantiomers was optimized offline using a proportional-differential (PD) controller. However, it turned out that this type of control concept was vulnerable to a delayed feedback, which plays an important role in on-line optimization and is the focus of the present work. Therefore, a different concept was applied. The concept is illustrated in Figure 3. The control unit consists of two parts: one is the parameter estimator and the other is the predictive optimizer based on the equilibrium-dispersion model introduced in Section 2.1. The estimator uses measured information from past switching cycles ( $\mathbf{H}_P$ ) to determine the axial dispersion coefficients and the isotherm parameters of the equilibrium-dispersion model by minimizing some weighted difference between the measured and the calculated concentrations in the product and the recycle streams.  $\mathbf{H}_D$  denotes some possible measurement delay, which is explicitly

taken into account in the remainder. The optimizer then uses the model with the updated parameters to minimize some weighted difference between the given reference values for the product purities and recycle concentration ratios at the end of some finite future horizon  $\mathbf{H}_F$  by calculating suitable flow-rates for the four zones of the SMB plant. Hereby, the switching time is fixed. Parameter estimation and predictive optimization are repeated from cycle to cycle to achieve convergence to the desired reference values.

For the solution of the partial differential equations (5) and the optimization, the initial conditions (i.e. the initial column profiles) at each cycle are required. In the present approach, they are calculated from the known initial conditions at the startup (empty columns) and then propagated from cycle to cycle. Plant model mismatch is compensated by the parameter estimator.

### 3.1. Estimation of process model parameters

To estimate the model parameters, the inverse method was applied with the parallelized Nelder-Mead simplex method [18], which is suitable to implement parallel computation and a gradient-free pattern search method with relatively fast convergence. The objective function to be minimized for parameter estimation is,

$$G(D_{a,i}, a_i, b_i) = \sum_{\forall i \in \mathbf{N}_S, \forall j \in \mathbf{N}_O, \forall k \in \mathbf{H}_P} \left( (c_{i,j,k}^{Exp})^{w_P} \left| \frac{c_{i,j,k}^{Cal} - c_{i,j,k}^{Exp}}{c_{i,j,k}^{Exp}} \right| \right) \quad (9)$$

where  $w_P$  is the power of weight factor,  $\mathbf{N}_O$  is the observed port set,  $\mathbf{H}_P$  is the control cycle set in the receding past horizon, the superscripts, *Cal* and *Exp* denote the values calculated by the process model and obtained from the process, respectively. The Nelder-Mead simplex method is a local optimization method, so that it may find sub-optimal points subject to the initial guesses. Nevertheless, it can be presumed that the estimated parameters can represent the process states quite well because the parameters are re-estimated in every control cycle exploiting the recently obtained process values including the newly obtained process outputs.

### 3.2. Predictive Optimization for Future Operations

With the updated process model parameters, the optimizer determines in each cycle suitable flow-rates for the four zones of the SMB plant by minimizing the following cost function for specified purities of the product and recycle streams,

$$H = \sum_{j \in \{Z1, \dots, Z4\}} H_j \quad (10-1)$$

$$H_{Z1} = \left( \frac{c_{S1,Rcyl,P_F}^{cal} - \hat{C}_{S1,Rcyl}}{\hat{C}_{S1,Rcyl,P_F}} \right)^2, \quad \hat{C}_{S1,Rcyl} = \hat{R}_{S1,Rcyl} \hat{C}_{S3,Raff} \quad (10-2)$$

$$H_{Z2} = \left( \frac{c_{S2,Extr,P_F}^{cal} - \hat{C}_{S2,Extr}}{\hat{C}_{S2,Extr}} \right)^2, \quad \hat{C}_{S2,Extr} = \frac{(1 - \hat{P}u_{Extr})}{\hat{P}u_{Extr}} \left( \sum_{i \in \mathbf{N}_S} c_{i,Extr,P_F}^{cal} - c_{S2,Extr,P_F}^{cal} \right) \quad (10-3)$$

$$H_{Z3} = \left( \frac{c_{S3,Raff,P_F}^{cal} - \hat{C}_{S3,Raff}}{\hat{C}_{S3,Raff}} \right)^2, \quad \hat{C}_{S3,Raff} = \frac{(1 - \hat{P}u_{Raff})}{\hat{P}u_{Raff}} \left( \sum_{i \in \mathbf{N}_S} c_{i,Raff,P_F}^{cal} - c_{S3,Raff,P_F}^{cal} \right) \quad (10-4)$$

$$H_{Z4} = \left( \frac{c_{S4,Rcyl,P_F}^{cal} - \hat{C}_{S4,Rcyl}}{\hat{C}_{S4,Rcyl}} \right)^2, \quad \hat{C}_{S4,Rcyl} = \hat{R}_{S4,Rcyl} \hat{C}_{S2,Extr} \quad (10-5)$$

Therein,  $\hat{C}$  is the desired average concentration at the end of the future control cycle,  $\hat{P}u$  is the desired product purity,  $\hat{R}$  is the desired impurity concentration ratio of the recycle stream to product stream.

The set point for  $R_{S1,Rcyl}$  and  $R_{S4,Rcyl}$  are discussed below in detail. The subscripts  $S1$ ,  $S2$ ,  $S3$ , and  $S4$  respectively denote the reference components for the zones 1 to 4, and the subscript  $P_F$  denotes the last control cycle of the future horizon. For a binary separation problem considered in this paper,  $S1$  and  $S3$  correspond to the more-retained component, and  $S2$  and  $S4$  correspond to the less-retained component. The specified control variables for the product stream purities,  $Pu_{Extr}$  and  $Pu_{Raff}$  represent the separation efficiencies of the zones 2 and 3, respectively. To obtain the desired product purities by controlling only the operating conditions of the zones 2 and 3, the regeneration efficiency in the zones 1 and 4, which determine the recycled impurities through the desorbent port, should be sufficiently high. This means that the concentrations in the recycle stream, the inlet stream of the zone 1 in this work, should not be higher than the acceptable impurity concentrations of the product streams [19, 20]. Therefore, the recycled component concentration ratios ( $R_{S1,Rcyl}$  and  $R_{S4,Rcyl}$ ) represent the regeneration efficiency of the zones 1 and 4, respectively. For example, the column in zone 1 is completely regenerated where  $R_{S1,Rcyl} = 0$ , or only partially regenerated where  $R_{S1,Rcyl} > 0$ . If  $R_{S1,Rcyl}$

$> 1$ , the column in zone 1 is not sufficiently regenerated and it is not possible to achieve the desired raffinate purity. Since all four cost functions are strongly coupled, each cost function cannot be separately optimized. A linear combination of all cost functions, Eq. (10-1) was minimized using the same search method, i.e. the Nelder-Mead simplex method.

Even though the optimizer uses an efficient PDE solver as discussed in Section 2, future prediction applied in rigorous model predictive control is still challenging. The operating conditions of every future control cycles can be different, i.e. the number of future operating conditions to be optimized is  $\{\text{four zone flow - rates}\} \times \{\text{number of future cycles}\}$ , to optimize the trajectory of controlled variables. However, the future operating conditions were all the same for future control cycles in this work, i.e. the number of future operating conditions to be optimized is just four zone flow-rates.

At the beginning of on-line optimization, an initial guess of operating conditions and model parameters are required. As illustrated in Figure 2, the basic properties, i.e. Henry's constants and the apparent dispersion coefficients, are obtained in the preliminary research to decide the suitable mobile and stationary phases. These values can be used for an approximate short-cut design [3] to provide suitable starting values of the operating conditions. After starting the process with these initially estimated operating conditions, the model parameters and operating conditions are updated 'switch-by-switch' with the control unit until the required product specifications are met.

Finally, in contrast to previous work mentioned in the introduction section, we do not directly optimize feed throughput or desorbent consumption. However, the introduction of  $R_{S1,Rcyl}$  and  $R_{S4,Rcyl}$  as additional controlled variables guarantees efficiency of zones 1 and 4 and thereby avoids unproductive solutions.

## 4. System Description

### 4.1. Implementation of control unit

Since the estimator required the process output from the process simulator and the optimizer provided updated optimal operating conditions to the process simulator, i.e. information should be consistently exchanged between the control unit and the process simulator, both were executed in this simulation study on the same platform (Intel i7, 4 cores, 8 threads, Microsoft Windows 7 OS). To implement the parallelized computation of the control unit, Microsoft Visual C++ Express Edition (Microsoft Inc. Ver. 2015) and its concurrent programming library, Parallel Pattern Library (Microsoft Inc.) were used. The SMB process to be controlled was simulated using Aspen Chromatography (Aspen Tech Inc. Ver. 8.8) applying the equilibrium-dispersion and linear driving for mass transfer models, Eqs. (1) and (2). The Windows Script Host automation using VBScript was used to communicate between the control unit and the SMB simulator.

#### 4.2. SMB simulation and performance criteria

For the simulation of the SMB process to be controlled, the model parameters for the separation of bicalutamide enantiomers were taken from our previous work [15]. The model parameters are listed in Table 1. To avoid any numerical dispersion effect in the simulation, a rather large number of nodes per column and the finite volume method (FVM) with an OSPRE flux limiter was used for the process simulator. An ideal process configuration that contains no system void volumes and consists of identical columns was considered. Therefore, the observed concentrations were the average concentrations in one control cycle (one port switching interval) as below.

$$C_{i,Extr,k}^{Exp} = \frac{\int_{t_k}^{t_k+t_c} c_{i,Extr,k}^{Sim} Q_{L,Extr} dt}{\int_{t_k}^{t_k+t_c} Q_{L,Extr} dt} \quad (11-1)$$

$$C_{i,Raff,k}^{Exp} = \frac{\int_{t_k}^{t_k+t_c} c_{i,Raff,k}^{Sim} Q_{L,Raff} dt}{\int_{t_k}^{t_k+t_c} Q_{L,Raff} dt} \quad (11-2)$$

$$C_{i,Rcyl,k}^{Exp} = \frac{\int_{t_k}^{t_k+t_c} c_{i,Z1n,k}^{Sim} Q_{L,Z1n} dt}{\int_{t_k}^{t_k+t_c} Q_{L,Z1n} dt} \quad (11-3)$$

where  $t_k$  is the time at the beginning of  $k^{\text{th}}$  control cycle,  $t_c$  is the elapsed time of one control cycle ( $= t_s$ ), and the superscript, *Sim* denotes the data obtained from the simulator. To determine the

optimized operation of the two regeneration zones, zones 1 and 4, the concentrations of the recycle stream (the inlet of the zone 1) were obtained together with the concentrations of the two outlet streams, c.f. Eqs. (10-2) and (10-5), which are essential for the optimized operation in zone 2 and 3.

While the process output can be immediately obtained at the end of the control cycle operation, i.e. the process output is not delayed in process simulation, intentional delayed process outputs were provided to the estimator to investigate the effect of delayed feedback. To compare the process performance, two performance factors, productivity and desorbent consumption (DC) were calculated as below,

$$Productivity = \frac{\{mass\ of\ (R)\ -\ bicalutamide\ in\ the\ extract\ stream\ for\ one\ control\ cycle\}}{\{Volume\ of\ adsorbent\}\{time\ of\ one\ control\ cycle\}} \quad (11-1)$$

$$DC = \frac{\{Volume\ of\ solvent\ used\ for\ one\ control\ cycle\}}{\{mass\ of\ (R)\ -\ bicalutamide\ in\ the\ extract\ stream\ for\ one\ control\ cycle\}} \quad (11-2)$$

## 5. Results

Table 2 shows the control unit parameters used in this work. For the parameter estimation, the estimator requires a certain number of past process outputs. Since the SMB system consists of four columns, from four to eight past cycles were used for the estimation. To test the robustness for delayed feedback, four different delay scenarios ( $\#H_D = 0, 1, 2, \text{ or } 4$ ) were tested with  $\#H_P = 6$  and  $\#H_F = 6$ . Corresponding to the numbers of delayed cycles, the control unit starts to control the process between the fourth cycle ( $\#H_D = 0$ ) and the eighth cycle ( $\#H_D = 4$ ) to get the same process outputs for all delay scenarios. As described in Eq. (10), the cost function for future prediction takes only the predicted process outputs at the end of the future horizon into account. Therefore, three different numbers of predicted future cycles were tested for control sensitivity ( $\#H_F = 2, 4, \text{ or } 6$ ). Because the extract impurity appears at the beginning of the next port switching interval, the minimum number of predicted future cycles was set to 2. Since the MC-AC scheme can provide well-approximated solutions with a small number of discrete cells, three different numbers of cells per column were also tested ( $\#N_C = 10, 20, \text{ or } 30$ ).

At the beginning of the SMB operation, the operating conditions were determined from the Henry's constants with the short-cut design method [3], and the initial apparent axial dispersion coefficients were arbitrarily set to  $1.0 \text{ cm}^2/\text{min}$  for both components. Consequently, the control unit takes the minimum information that can be obtained from the preliminary small-scale research (the first step in Figure 2). The estimator conducted 100 iterations of the pattern search at each control cycle without any tolerance set. This means that the control unit consumes more or less the same time for the parameter estimation. The tolerance for the optimizer was set to 0.001 with the same number of iterations, 100.

### **5.1. Standard mode of SMB operation – robustness and sensitivity**

Figure 4a shows the robustness of the controller when a wrong model for the adsorption isotherm is used for the optimization, i.e. Langmuir instead of bi-Langmuir (plant-model mismatch). Since the initial operating conditions were determined from the short-cut method based on the equilibrium model, the flow-rates of zones 1 and 2 are equal to the flow-rates of the zones 3 and 4, respectively. Although the simulated SMB process obeys the bi-Langmuir isotherms, the control units with both Langmuir and bi-Langmuir isotherms with 10 to 30 cells per column can find the same optimized operating conditions with similar convergence. However, the estimated dispersion coefficients deviate when a small number of cells was taken for the process model ( $\#N_c = 10$  in Table 3). Especially the apparent dispersion coefficient of (R)-bicalutamide was close to zero and much smaller than the dispersion coefficient applied in the process simulation (cf. Table 1) to form sharp shock front in the sparse number of cells (the upper profiles in Figure 5). Since both Langmuir and bi-Langmuir isotherms provide smooth-concave isotherm curves, the control unit can estimate similar isotherm parameters, and the estimated internal concentration profiles were well matched compared to the process (the middle and lower profiles in Figure 5). When the Langmuir model (mismatched isotherm model) was applied for the control, the shock front of the more-retained (R)-bicalutamide, which is located in the middle of the less-retained component elution band, was not precisely estimated compared to the bi-Langmuir model. When sufficient numbers of cells and correct isotherm

models were applied (bi-Langmuir with  $\#N_C = 20$  and 30 in Table 3), the isotherm parameters and apparent dispersion coefficients were matching well with the plant parameters used in the process simulation (Table 1). This means that the parameter estimation provides physically meaningful values, and the correct process model should be determined in the second step of the design campaign (Figure 2).

For further robustness and sensitivity test, the bi-Langmuir isotherms and  $\#N_C = 20$  was chosen for the on-line optimization. Figure 4b shows the robustness of the control unit with various delayed feedback scenarios. The control unit estimated the process parameters that can precisely describe the process behavior and used them to predict the current process state, so that the control unit provided the same pattern of convergence even when one complete SMB cycle (4 port switching intervals = 4 control cycles) was delayed. To estimate the model parameters, the control unit requires a certain number of past process outputs. In this simulation study, all columns were identical and no system void volume was considered, so that the convergence and sensitivity of the control unit were not significantly changed as  $\#H_P$  was varied from 4 to 8 (Figure 4c). In all above mentioned cases, the length of the future horizon,  $\#H_F$  was set to 6. Because of the relatively long future horizon, almost cyclic steady-state is reached and the control unit has low sensitivity. The operating conditions converged to the optimum values in 4 cycles after the control unit starts. However, it took around 16 cycles for the purities of products to converge. Figure 4d shows that the control sensitivity can be improved by reducing the length of the future horizon. When  $\#H_F = 2$ , the purities of products could converge in 5 cycles, which is 3 times faster than for  $\#H_F = 6$ .

Figure 6 shows the robustness of the control unit for set-point changes. At the end of every 40<sup>th</sup> cycles, the set product purities were changed with constant recycle concentration ratios,  $R_{Rcyl}$  (Figures 6a, 6b, and 6c) or the set recycle concentration ratios were changed with fixed product purities (Figure 6d). For favorable isotherms the purity of the raffinate product is determined by the shock position of the more-retained solute elution band in the zone 3 and the purity of extract is determined by the position of the dispersive wave of the less-retained solute elution band in the zone 2 as shown in Figure 5. Therefore, a very slight change of  $Q_{L,Z3}$  resulted in a significant change of the

raffinate purity (80<sup>th</sup> and 160<sup>th</sup> cycles in Figures 6a, 6b, and 6c). Since the  $R_{S1,Rcyl}$  and  $R_{S4,Rcyl}$  values are respectively related to the impurity concentrations in the raffinate and extract ports,  $Q_{L,Z1}$  and  $Q_{L,Z4}$  were correspondingly changed where the reference purity values were changed (Figures 6a, 6b, and 6c). However, the flow-rates of the zones 2 and 3,  $Q_{L,Z2}$  and  $Q_{L,Z3}$  were not changed much when the  $\hat{R}_{S1,Rcyl}$  and  $\hat{R}_{S4,Rcyl}$  values were changed because the impurity concentrations in the recycle stream were not significantly changed in complete separation (99% of purities) even though  $\hat{R}_{S1,Rcyl}$  and  $\hat{R}_{S4,Rcyl}$  values were jumping from 0.1 to 0.9 (Figures 6d). All controlled variables converged in 10 control cycles (20 control cycles for the raffinate purity), and well maintained. Since the control unit took four controlled variables that can represent the performance of the four zones (two product purities and two recycled concentration ratios), the control unit found only one optimized operating condition.

As discussed in the explanation of Figure 5, the Langmuir isotherms also provides quite good estimated internal concentration profiles. The control histories for both Langmuir and bi-Langmuir isotherms are compared in Figure 6b. The control concept relies on concentration measurement at the two product ports and the desorbent port. Concentrations at the feed port were not measured to avoid remixing due to the extra volume which would be required to collect the samples at the feed port. Therefore, the control unit has to estimate the internal concentration profiles around the feed port without proper information, and therefore, the mismatched isotherm model provides poor profile estimation around the feed port (Figure 5, between 2 to 3 of axial distance), and an unwanted overshoot/undershoot appeared where wrong isotherm model were applied (Figure 6b). A reduced future horizon can increase the control sensitivity as shown in Figure 6c. When  $\#H_F = 2$ , the control sensitivity was significantly increased. The controlled variables converged to the set-point in several control cycles. The zone flow-rates were steeply varied right after the set-point disturbance. Therefore, the length of the future horizon should be determined according to the system conditions, and rigorous nonlinear model predictive control that calculates different operating conditions in every future control cycles may provide better performance. This, however, was not considered in this work because of the high computational load.

By changing the set points for the desired purities ( $Pu_{Extr}$  and  $Pu_{Raff}$ ) and the regeneration conditions ( $R_{S1,Rcyl}$  and  $R_{S4,Rcyl}$ ), the process performance, i.e. productivity and desorbent consumption, was also evaluated. The set purities were changed from 99% (complete separation) to 70% for both products and for the target ( $Pu_{Extr}$ ) or waste ( $Pu_{Raff}$ ) products. The corresponding process performance in terms of productivity and desorbent consumption is shown in Figure 7a as a function of product purities. Each optimized operating conditions were obtained by the dynamic optimizing control in 40 cycles, and all conditions were done in one simulation run. Corresponding to the purity criteria, the optimized operating conditions can be compared to design an appropriate process. For example, the reduced waste purity condition (reduced yield of the target component; points A and B in Figure 7a) consumes 21% less desorbent, but productivity decreased to 82% compared to the complete separation condition. The black circles in Figure 7a indicate an increased productivity with an increasing purity of the raffinate waste stream. This can be rationalized in the following way: As the raffinate purity increases, the recovery of the target component in the extract also increases but the feed throughput decreases. In this case, the first effect is slightly dominant over the second effect, so that in total the productivity is slightly increasing. Figure 7b shows the changes of productivity and desorbent consumption by the regeneration conditions,  $\hat{R}_{S1,Rcyl}$  and  $\hat{R}_{S4,Rcyl}$ . As the set concentration ratio in the recycle stream increased, the productivities were linearly decreased. However the desorbent consumptions were steeply increased as the process required relatively better regeneration conditions ( $R_{S1,Rcyl}$  and  $R_{S4,Rcyl} < 0.2$ ).

## 5.2. Advanced SMB operating modes

Figure 8a shows the extract and raffinate stream histories at CSS for three different introduced operating modes (Std: standard, OSS: outlet stream swing, and FF: flow focusing). In the standard operation, all zone flow-rates are constant for one port switching interval, so that the flow-rates of the product streams are also constant.

In the OSS operation, one product stream is closed when rich impurity profiles tend to be eluted (at the beginning of the port switching interval for the extract stream and at the end of the port switching interval for the raffinate stream), and the other stream flow-rate is increased to hold the balance of the in- and out-flows. If the operation factor is greater than zero, both product streams are opened in a certain portion of the port switching interval, and the SMB process is operated as the standard operation in this portion of the switching interval.

In the FF operation, all external flows are focused in the middle of the port switching interval, and the flow-rates are inversely proportional to the operation factor to have the same average flows as the corresponding standard operation. The liquid phase is internally circulated while all external flows are closed. Therefore, rich impurity profiles and diluted product profiles at both extract and raffinate ports are not eluted but transferred to the next column for further separation and enrichment.

In the standard operation, the zones 2 and 4 should not be contaminated by the impurities of the extract and the raffinate streams at the end of the port switching interval (upper graph in Figure 8b) to reach the desired high product purity. Therefore, the mixture band from the rear end of less-retained solute to the front end of more-retained solute should be placed in zone 3. On the contrary, the mixture band of the OSS and FF operations can be wider than that of the standard operation since the impurity concentration profiles can penetrate into the zones 2 and 4 at the end of the port switching interval (middle and lower graphs in Figure 8b). This results in higher feed throughput for the same product purities, so that the productivity (48% higher than the standard operation) and desorbent consumption (20% and 33% less than the standard operation, respectively) can be improved in the OSS and FF operations as shown in Figure 9a.

Since the FF operation intermittently suspends all external flows including the feed and desorbent flows, the FF operation can reduce the desorbent flow. In contrast, the OSS operation requires more desorbent to achieve the same product quality (Figure 9b). The FF operation enriches the product concentration. Both advanced operating modes can be applied in the conventional SMB process with simple on/off of the external flows. The main purpose of these intermittent flow control is adjusting the internal concentration profiles in right position before collecting products. Therefore,

the FF operation that allows the inlet flows to intermit can achieve higher productivity and lower desorbent consumption than the OSS operation.

### 5.3. Computational aspects

The control unit took the average concentrations from three observation ports, the extract, raffinate, and desorbent ports. This means that the effluents at these three ports should be stored for one control cycle and be analyzed at the end of the control cycle. To obtain individual concentrations of a mixture, a proper analysis method that may require a certain time should be applied, so that the computation time should be much shorter than the control cycle. This is also the reason why the port switching interval is constant. Figure 10a shows the elapsed computation time and the number of simulations that were performed in one control cycle. At the beginning, the initial model parameters and the operating conditions were obtained from the Henry's constants, so that a large number of simulations (3000 to 4000) was required. Once the control unit finds good model parameters and optimized operating conditions, the required number of simulations was decreased to about 2000. For up to 30 cells per column conditions, the elapsed computation times were less than 3 min. Therefore, the control unit can finish all computations within one control cycle (= 4 min, one port switching interval) provided where the analysis unit is fast enough.

As mentioned above, the estimator uses a fixed and relatively small number of iterations for the parameter estimation (100 iterations) to finish all computation within a designated time compared to the number of parameters to be estimated (7 parameters for bi-Langmuir isotherms), so that the estimator may not have enough time to obtain well estimated model parameters. However, the estimator finds better model parameters in every control cycle, and finally finds the model parameters as illustrated in Figure 10b with a high convergence rate during the first 20 cycles.

The chosen model system is a typical preparative chromatography, so that the column efficiency, the average number of theoretical plates (NTP) calculated from the dispersion coefficient ( $= L_c \bar{u}_L / 2D_L$ ) is around 500 and the less-retained component does not have strong interaction with the

adsorbent surface, which leads to the formation of dispersed shock fronts in zones 3 and 4. To test the performance of the control unit for various efficiency systems, a new model system with up to 7500 theoretical plates with Langmuir isotherms was chosen (Table 4). To avoid any plant-model mismatch, the same equilibrium-dispersion model was chosen for the plant and the control unit. The feed concentrations of both solutes A and B were fixed to 10 g/L, so that this system is strongly nonlinear (the nonlinearity factor,  $1 + b_{AC_{Feed,A}} + b_{bC_{Feed,b}} = 2.5$ ). This means that the shock front is steeper as the axial dispersion coefficient decreases (the number of theoretical plates increases), and it is difficult to find the right cut position for the raffinate product ( $Q_{L,Z3}$ ) and desorbent regeneration ( $Q_{L,Z4}$ ). It took more control cycles to converge the raffinate purity to the set purity (Figure 11a). The control unit with up to 40 cells per column could control the system up to 7500 theoretical plates. Compared to the theoretical plates of the plant the required numbers of cells for the optimizing control were two orders of magnitude smaller because the MC-AC scheme can compensate the numerical dispersion which is introduced by a low number of cells and can reproduce steep fronts with a rather low number of cells [14]. The model parameters estimated by the control unit were close to the true plant parameters. Especially, the relative standard deviation of the isotherm parameters is 2.9%. Even though the estimated dispersion coefficients in the second and fourth cases were quite different (the relative standard deviation is 37.8% for all cases and 8.1% for the first and third cases), the estimated internal concentration profiles were well matching the simulated process profiles (Figure 11b).

## 6. Conclusions

In this work, we presented a new concept for the on-line optimization of SMB processes. It relies on on-line measurements of product and recycle concentrations and a rigorous nonlinear process model. The concept was tested thoroughly *in silico* for three different operational modes of the SMB process. It was shown that the on-line optimization can determine suitable operating conditions to meet the given purity and recycle requirements from rough initial guesses. It is seen as a promising alternative to shorten expensive offline design procedures.

An extensive experimental validation of the on-line optimization concept is presented in a second part considering the separation of two bicalutamide enantiomers as a case study [21].

## References

- [1] D. B. Broughton, R. W. Neuzil, J. M. Pharis, C. S. Brearby, The parex process for recovering paraxylene, *Chem. Eng. Prog.* 66 (1970) 70-75.
- [2] K.-M. Kim, J. W. Lee, S. Kim, F. V. Santos da Silva, A. Seidel-Morgenstern, C.-H. Lee, Advanced operating strategies to extend the applications of simulated moving bed chromatography, *Chem. Eng. Technol.* 40 (2017) 2163-2178.
- [3] G. Storti, M. Mazzotti, M. Morbidelli, S. Carrà, Robust design of binary countercurrent adsorption separation processes, *AIChE J.* 39 (1993) 471-492.
- [4] Z. Ma, N.-H. L. Wang, Standing wave analysis of smb chromatography: linear systems, *AIChE J.* 43 (1997) 2488-2508.
- [5] K. B. Lee, R. B. Kasat, G. B. Cox, N.-H. L. Wang, Simulated moving bed multiobjective optimization using standing wave design and genetic algorithm, *AIChE J.* 54 (2008) 2852-2871.
- [6] J. W. Lee, P. C. Wankat, Design of pseudo-simulated moving bed process with multi-objective optimization for the separation of a ternary mixture: Linear isotherms, *J. Chromatogr. A*, 1217 (2010) 3418-3426.
- [7] A. Toumi, S. Engell, Optimization-based control of a reactive simulated moving bed process for glucose isomerization, *Chem. Eng. Sci.* 59 (2004) 3777-3792.
- [8] A. Toumi, S. Engell, M. Diehl, H. G. Bock, J. Schlöder, Efficient optimization of simulated moving bed processes, *Chem. Eng. Process.* 46 (2007) 1067-1084.
- [9] G. Erdem, S. Abel, M. Morari, M. Mazzotti, M. Morbidelli, J. H. Lee, Automatic control of simulated moving beds, *Ind. Eng. Chem. Res.* 43 (2004) 405-421.

- [10] C. Grossmann, G. Erdem, M. Morari, M. Amanullah, M. Mazzotti, M. Morbidelli, 'Cycle to cycle' optimizing control of simulated moving beds, *AIChE J.* 54 (2008) 194-208.
- [11] C. Grossmann, C. Langel, M. Mazzotti, M. Morbidelli, M. Morari, Multi-rate optimizing control of simulated moving beds, *J. Process Control* 20 (2010) 490-505.
- [12] S. Engell, A. Toumi. Process Control. In: *Preparative Chromatography (2nd Edition)*, Eds: H. Schmidt-Traub, M. Schulte, A. Seidel-Morgenstern, Wiley VCH, Weinheim, 2012.
- [13] S. Engell, A. Kienle. Process Control. In: *Preparative Chromatography (3rd Edition)*, Eds: H. Schmidt-Traub, M. Schulte, A. Seidel-Morgenstern, Wiley VCH, Weinheim, 2020, in press.
- [14] J. W. Lee, A. Seidel-Morgenstern, Solving hyperbolic conservation laws with active counteraction against numerical errors: Isothermal fixed-bed adsorption, *Chem. Eng. Sci.* 207 (2019) 1309-1330.
- [15] H. Kaemmerer, Z. Horvath, J. W. Lee, M. Kaspereit, R. Arnell, M. Hedberg, B. Herschend, M. J. Jones, K. Larson, H. Lorenz, and A. Seidel-Morgenstern, Separation of racemic bicalutamide by an optimized combination of continuous chromatography and selective crystallization, *Org. Process Res. Dev.* 16 (2012) 331-342.
- [16] P. S. Gomes, A. E. Rodrigues, Outlet streams swing (OSS) and multifeed operation of simulated moving beds, *Sep. Sci. Technol.* 42 (2007) 223-252.
- [17] S. Katsuo, M. Mazzotti, Intermittent simulated moving bed chromatography: 1. Design criteria and cyclic steady-state, *J. Chromatogr. A* 1217 (2010) 1354-1361.
- [18] D. Lee, M. Wiswall, A parallel implementation of the simplex function minimization routine, *Comput. Econ.* 30 (2007) 171-187.
- [19] J. W. Lee, A Seidel-Morgenstern, Model predictive control of simulated moving bed chromatography for binary and pseudo-binary separations: Simulation study, *IFAC-PapersOnLine* 51 (2018) 530-535.

- [20] J. W. Lee, P. C. Wankat, Optimized design of recycle chromatography to isolate intermediate retained solutes in ternary mixtures: Langmuir isotherm systems, *J. Chromatogr. A* 1216 (2009) 6946–6956.
- [21] J. W. Lee, A. Kienle, A. Seidel-Morgenstern, On-line optimization of four-zone simulated moving bed chromatography using an equilibrium-dispersion model: II. Experimental validation, Submitted to *Chem. Eng. J.*

## Appendix A: Advanced SMB operation

### Outlet Stream Swing (OSS) operation

In the ref. [16], the authors have considered two types of two-step OSS operations, the raffinate-to-extract operation as shown in Figure A1a and the extract-to-raffinate operation (the opposite step order). The former provides better purities than the latter and the standard SMB operation. Therefore, we applied the raffinate-to-extract operation. As the authors in the ref. [16] mentioned, we took the intermediate step, the step 2 in Figure A1b to operate the transient conditions between the conventional SMB operation and the pure OSS operation. If the operation factor,  $F_{Op}^{OSS} = 1$ , the steps 1 and 3 are omitted, so that the operation mode is the same as the conventional SMB operation. On the contrary, the step 2 is omitted and the operation mode is the pure OSS operation if  $F_{Op}^{OSS} = 1$ .

In this work, the feed and desorbent flow-rates were fixed during the port switching interval. It means that the raffinate and extract flow-rates are the same during one of the product streams is open in the step 1 or 3. Therefore, the operation times of the steps 1 and 3 were determined by the operation factor,  $F_{Op}^{OSS}$  and the corresponding conventional SMB operation as described in Eq. (7). Consequently, this OSS operation has one more degree of freedom than the conventional SMB operation, so that it has leeway to provide better process performance than the conventional SMB operation.

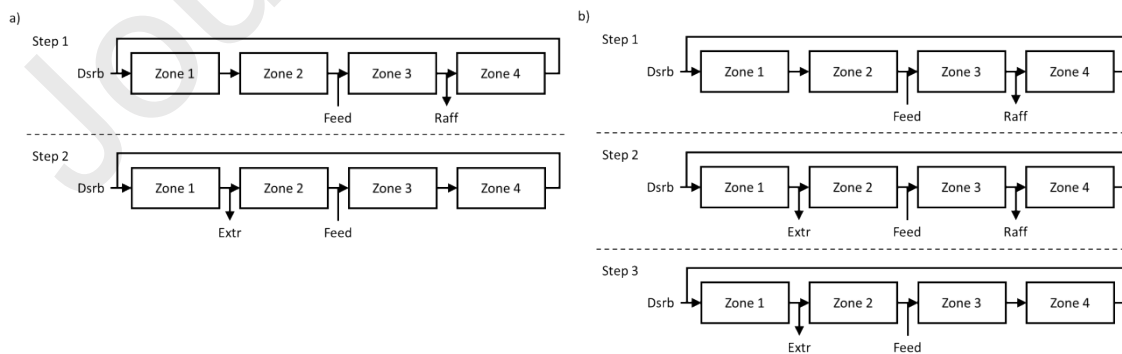


Figure A1. Schematic flow diagram of the outlet stream swing operation. a) Two-step operation proposed in [16]; b) Three-step operation applied in this work.

### Flow-Focusing (FF) operation

The authors in the ref. [17] proposed the SMB operation with intermittent external flow operation as shown in Figure A2a. In step 2, there is no external flows, but the zone flows are internally circulated to position the internal profiles in proper place. Then the well-posed profiles are harvested in the next step 1 with open-loop three-zone SMB operation. In this work, we proposed similar operation mode called the flow-focusing (FF) operation.

With the same manner applied in the OSS operation, we added one more internal circulation step at the beginning as shown in Figure A2b. Then the harvesting step, the step 2 is located in the middle of the port switching interval, and the external flows are focused in the step 2 operation. As described in Eq. (8), this operation mode has two factors for the operation,  $F_{Op}^{FF}$  and  $F_{Pos}^{FF}$ . The former indicates the length of the step 2 and the latter indicates the position of the step 1. Therefore, this FF operation has two more degree of freedom than the conventional SMB operation and even one more degree of freedom than the OSS operation. It means that the FF operation has a big potential to improve the process performances.

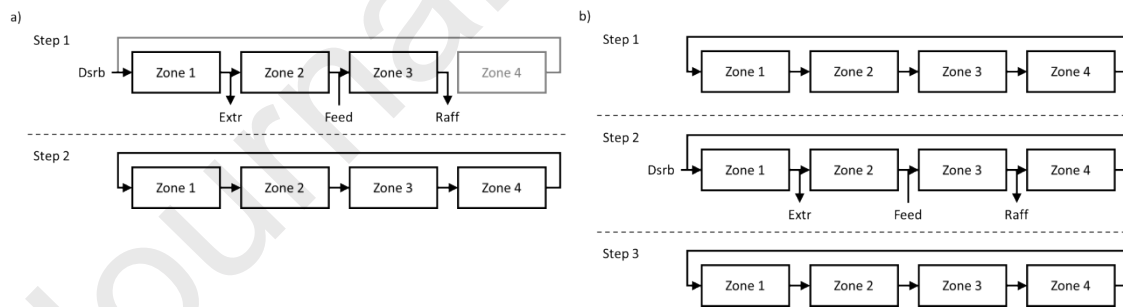


Figure A2. Schematic flow diagram of the intermittent-SMB [17] (a) and the flow-focusing operation. In the gray zone and stream, flows are zero.

## List of Tables

- Table 1. Process specifications, numerical methods, and model parameters of the system used for the SMB process simulation [15].
- Table 2. Number of receding horizon cycles, process variables, initial process model parameters, and Nelder-Mead method parameters used for the on-line optimization of the SMB process.
- Table 3. Average apparent dispersion coefficients and adsorption isotherm parameters estimated by the on-line control unit for the last four control cycles of Figure 4a.
- Table 4. Model parameters for the process simulation and average model parameters estimated by the on-line control unit for the last four control cycles of Figure 11.

## List of Figures

- Figure 1. Schematic illustration of closed-loop four-zone simulated moving bed process with two columns per zone configuration.  
Schematic flow diagram (upper);  
Well-posed internal concentration profiles at the middle of port switching interval (lower).
- Figure 2. Comparisons of the conventionally applied and the proposed design steps for the SMB process.
- Figure 3. Schematic block-diagram of (a) the on-line optimization and (b) the receding horizons.
- Figure 4. Comparisons of control histories of zone flow-rates (process input) and purities (controlled variables).  
a) For Langmuir and bi-Langmuir isotherms and various numbers of cells;  
b) For various lengths of the delayed horizon;  
c) For various lengths of the past horizon;

d) For various lengths of the future horizon.

Standard control condition: bi-Langmuir,  $\#N_C = 20$ ,  $\#H_P = 6$ ,  $\#H_D = 1$ ,  $\#H_F = 6$ .

Figure 5. Comparison of internal concentration profiles of process and control unit at the end of the control cycle in Figure 4a.

a) Langmuir isotherms; b) bi-Langmuir isotherms.

Figure 6. Control histories of zone flow-rates (process input) and purities (controlled variables) with set point changes.

a) Product purities;

b) Product purities, comparisons of Langmuir and bi-Langmuir isotherms;

c) Product purities; comparisons of  $\#H_F = 6$  and  $\#H_F = 2$ ;

d) Recycle stream concentration ratios.

Standard control condition: bi-Langmuir,  $\#N_C = 20$ ,  $\#H_P = 6$ ,  $\#H_D = 1$ ,  $\#H_F = 6$ .

Figure 7. Changes of productivity and desorbent consumption as a function of purity set points for  $R_{S1,Rcyl} = R_{S4,Rcyl} = 0.25$  (a) and as a function of recycle stream concentration ratio set points for the product purity set points given in the diagram (b).

Control condition: bi-Langmuir,  $\#N_C = 20$ ,  $\#H_P = 6$ ,  $\#H_D = 1$ ,  $\#H_F = 6$ .

Figure 8. Comparisons of product port histories at CSS (a) and internal concentration profiles at the end of CSS cycle (b) for different operating modes.

Std: standard operation; OSS: outlet stream swing operation; FF: flow focusing operation;

$F_{Op} = 0.5$ .

Arrows denote the observed range by average extract and raffinate process outputs (a) and corresponding internal concentration profiles (b).

Figure 9. Improvement of productivity and desorbent consumption by the OSS and FF operating modes.

$Pu_{Extr} = Pu_{Raff} = 99\%$ ;  $R_{S1,Rcyl} = R_{S4,Rcyl} = 0.25$ ;

Standard operation:  $F_{Op} = 1.0$

Figure 10. Computational performances of the control unit in terms of the number of simulations conducted and the elapsed computation time (a) and the trace of the objective function for the parameter estimation (b).

$$Pu_{Extr} = Pu_{Raff} = 99\%; R_{S1,Rcyl} = R_{S4,Rcyl} = 0.25; F_{Op} = 0.5;$$

$\bar{t}_{Sim}$ : average elapsed time for one port switching internal simulation in the control unit.

Figure 11. Comparisons of the control histories (a) and the internal concentration profiles of the process and the control unit (b) with various column efficiencies in Table 4.

Table 1.

System	Four-zone closed-loop SMB
Columns per zone (Zone 1 / Zone 2 / Zone 3 / Zone 4)	1 / 1 / 1 / 1
PDE solver	FVM with OSPRE flux limiter
# of column nodes	200
Column	ChiralPak AD, 20 $\mu$ m
I.D. [cm] $\times$ Length [cm]	2.5 $\times$ 10.0
Porosity [-]	0.69
Mobile Phase	Methanol
Feed	Bicalutamide racemates
Concentration [g/L]	20 (10 for each)
Isotherms	Bi-Langmuir
$q_{1,Max}$ [g/L]	43.3
$K_{1,(R)}$ [g/L] / $K_{1,(S)}$ [g/L]	0.010 / 0.010
$q_{2,Max}$ [g/L]	15.0
$K_{2,(R)}$ [g/L] / $K_{2,(S)}$ [g/L]	0.224 / 0.006
Dispersion	Constant dispersion
Dispersion coefficient, $D_L$ [cm <sup>2</sup> /min]	0.730
Mass Transfer	Solid film, linear lumped
$k_{eff,(R)}$ [1/min] / $k_{eff,(S)}$ [1/min]	245.9 / 58.8

Table 2.

Cycles	
# of past cycles for estimation, # $\mathbf{H}_P$	4, <u>6</u> , 8
# of delayed cycles, # $\mathbf{H}_D$	0, <u>1</u> , 2, 4
# of predicted future cycles, # $\mathbf{H}_F$	2, 4, <u>6</u>
Control cycle	One port switching interval, 3 min
Variables	
# of cells per column, # $\mathbf{N}_C$	10, 20, 30
Process inputs	$Q_{L,Z1}, Q_{L,Z2}, Q_{L,Z3}, Q_{L,Z4}$
Process outputs	$\bar{c}_{i, Extr}, \bar{c}_{i, Raff}, \bar{c}_{i, Rcycl}$
Controlled variables	$Pu_{Extr}, Pu_{Raff}, R_{S1,Rcycl}, R_{S4,Rcycl}$
Set-points	70 ~ 99%, 70 ~ 99%, 0.01 ~ 1.0, 0.01 ~ 1.0
S1, S3	(R)-bicalutamide
S2, S4	(S)-bicalutamide
Initial process parameters	
Henry's constants, $a_{(R)} / a_{(S)}$ <sup>1)</sup>	3.8/0.54
Apparent dispersion coefficients $D_{a,(R)} / D_{a,(S)}$ <sup>2)</sup>	1.0/1.0
Max. # of iteration / Tolerance	
Estimator	100 / -
Optimizer	50 / 0.001

<sup>1)</sup> From the isotherm parameters in Table 1,  $a_i = q_{1,Max}K_{1,i} + q_{1,Max}K_{1,i}$

<sup>2)</sup> Arbitrary chosen from the dispersion coefficient in Table 1 [cm<sup>2</sup>/min]

Table 3.

	$\#N_C$	$D_{a,(R)}$	$D_{a,(S)}$	$q_{Max}$	$K_{(R)}$	$K_{(S)}$		
Langmuir	10	0.150	1.123	21.90	1.81e-1	3.16e-2		
	20	1.025	1.505	23.35	1.55e-1	2.96e-2		
	30	1.023	1.466	23.23	1.56e-1	3.02e-2		
	$\#N_C$	$D_{a,(R)}$	$D_{a,(S)}$	$q_{1,Max}$	$K_1$	$q_{2,Max}$	$K_{2,(R)}$	$K_{2,(S)}$
Bi-Langmuir	10	0.005	0.761	27.11	1.87e-2	14.48	2.46e-1	7.73e-4
	20	0.920	1.113	26.53	1.97e-2	14.56	2.19e-1	1.71e-3
	30	0.852	1.047	50.65	9.71e-3	14.33	2.30e-1	1.44e-3

Table 4.

Process <sup>1)</sup>			Controller <sup>2)</sup>						
$D_L$	$\overline{NTP}^3)$	$q_{Max}; K_A; K_B$	$N_C$	$D_{a,A}$	$D_{a,B}$	$q_{Max}$	$K_A$	$K_B$	Speed <sup>4)</sup>
0.5	792	40; 0.1; 0.05	10	0.498	0.489	39.93	0.1001	0.0498	24.3; 115.5
0.25	1543		20	0.024	0.239	38.01	0.1084	0.0530	25.2; 118.8
0.1	3775		40	0.116	0.086	40.23	0.0986	0.0494	100.3; 863.0
0.05	7475		40	0.006	0.019	39.84	0.1007	0.0506	96.4; 558.7

<sup>1)</sup> Langmuir isotherms (A: more-retained, B: less-retained); all other process parameters are the same as Table 1.

<sup>2)</sup> Average estimated parameters in the last four control cycles.

<sup>3)</sup> Average number of theoretical plates,  $\overline{NTP} = L_c \bar{u}_L / 2D_L$ ,  $\bar{u}_L = \frac{1}{4}(u_{L,Z1} + u_{L,Z2} + u_{L,Z3} + u_{L,Z4})$

<sup>4)</sup> Average one cycle simulation time [ms/cycle]; Max. elapsed time for the controller computation [s]

Figure 1.

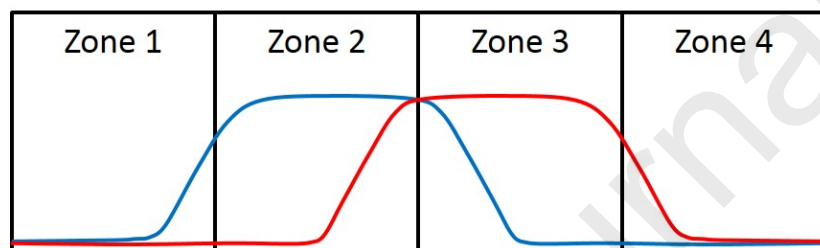
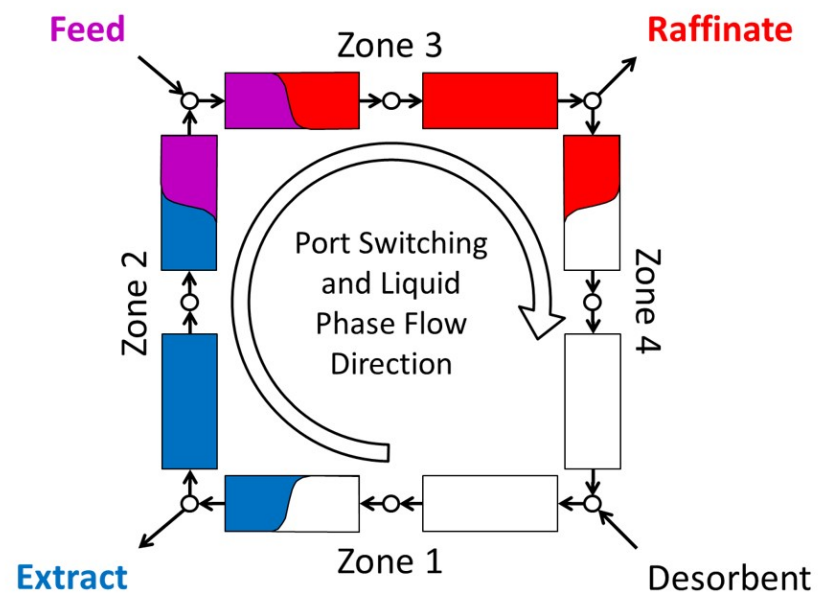


Figure 2.

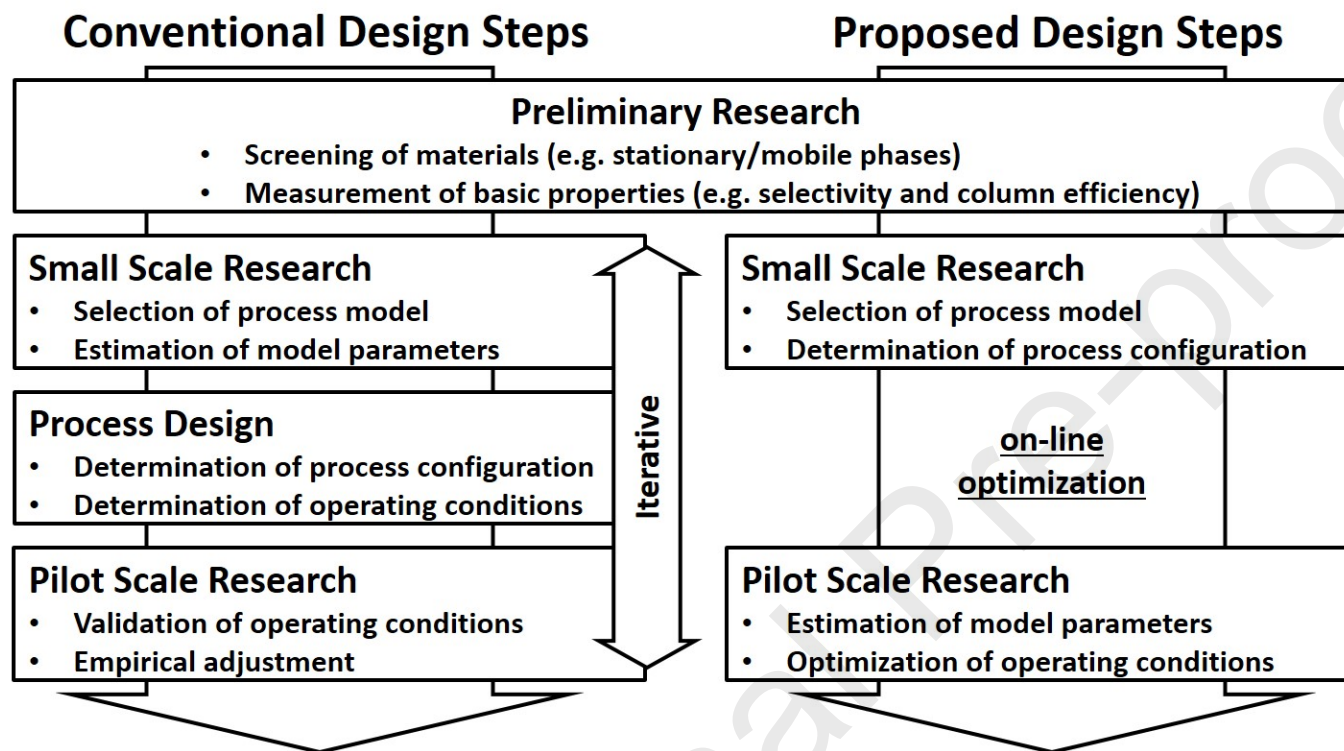


Figure 3.

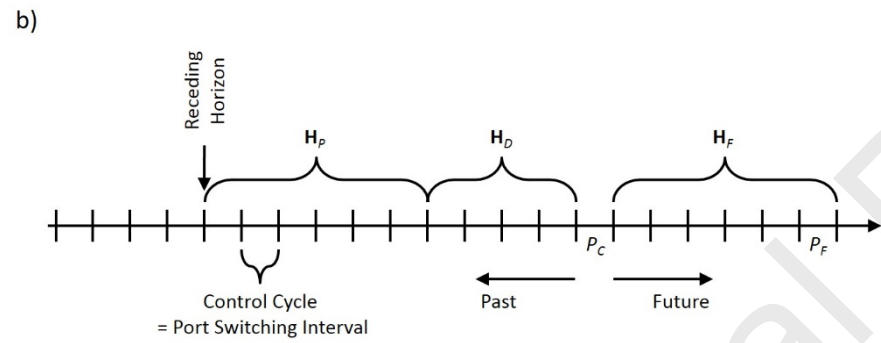
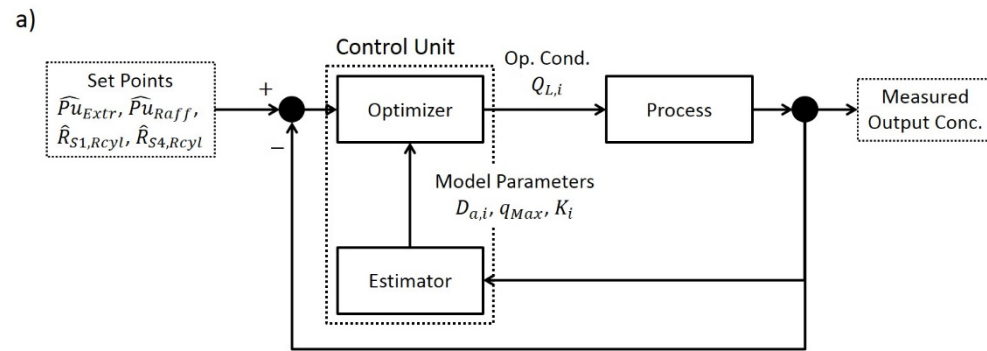


Figure 4.

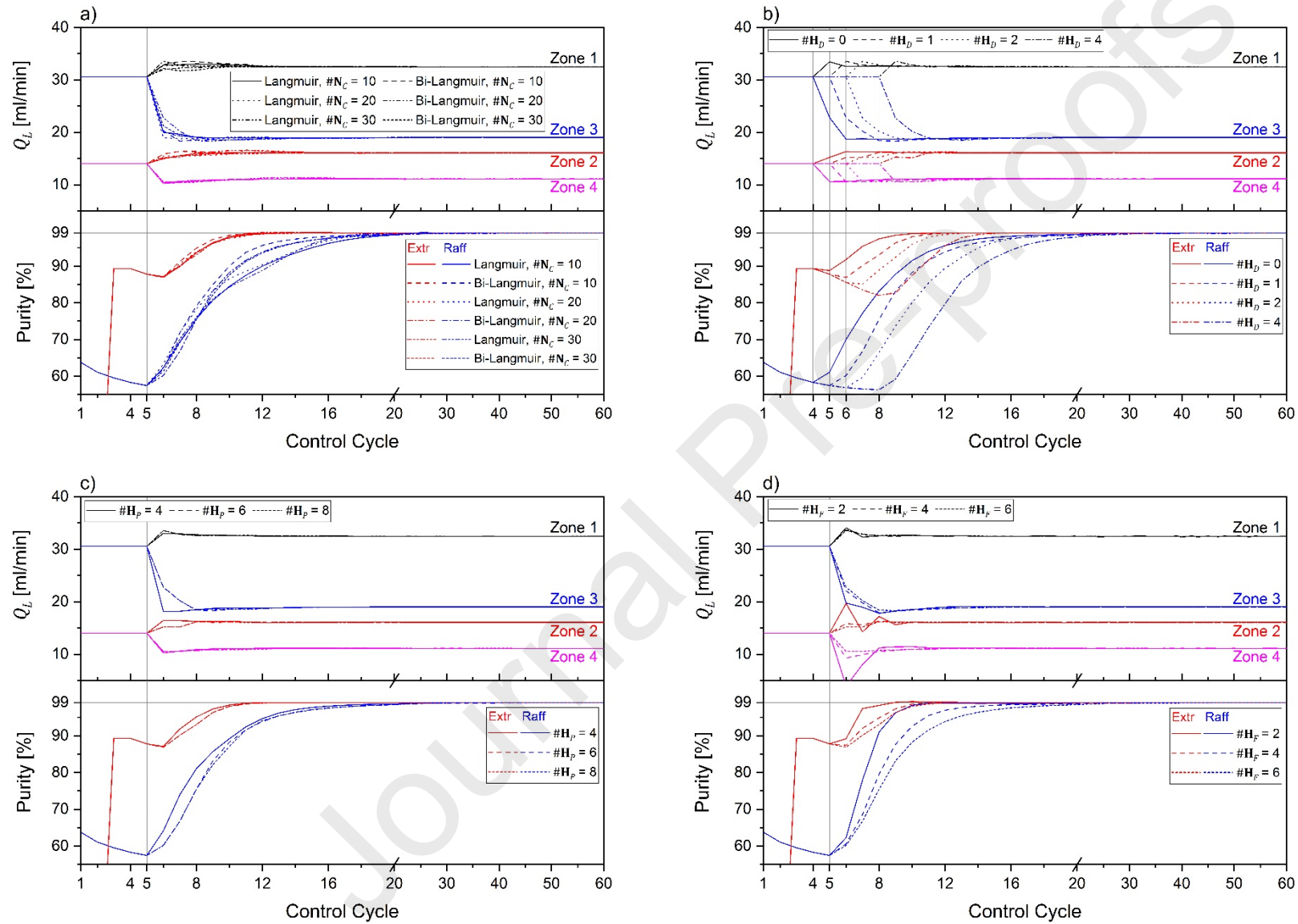


Figure 5

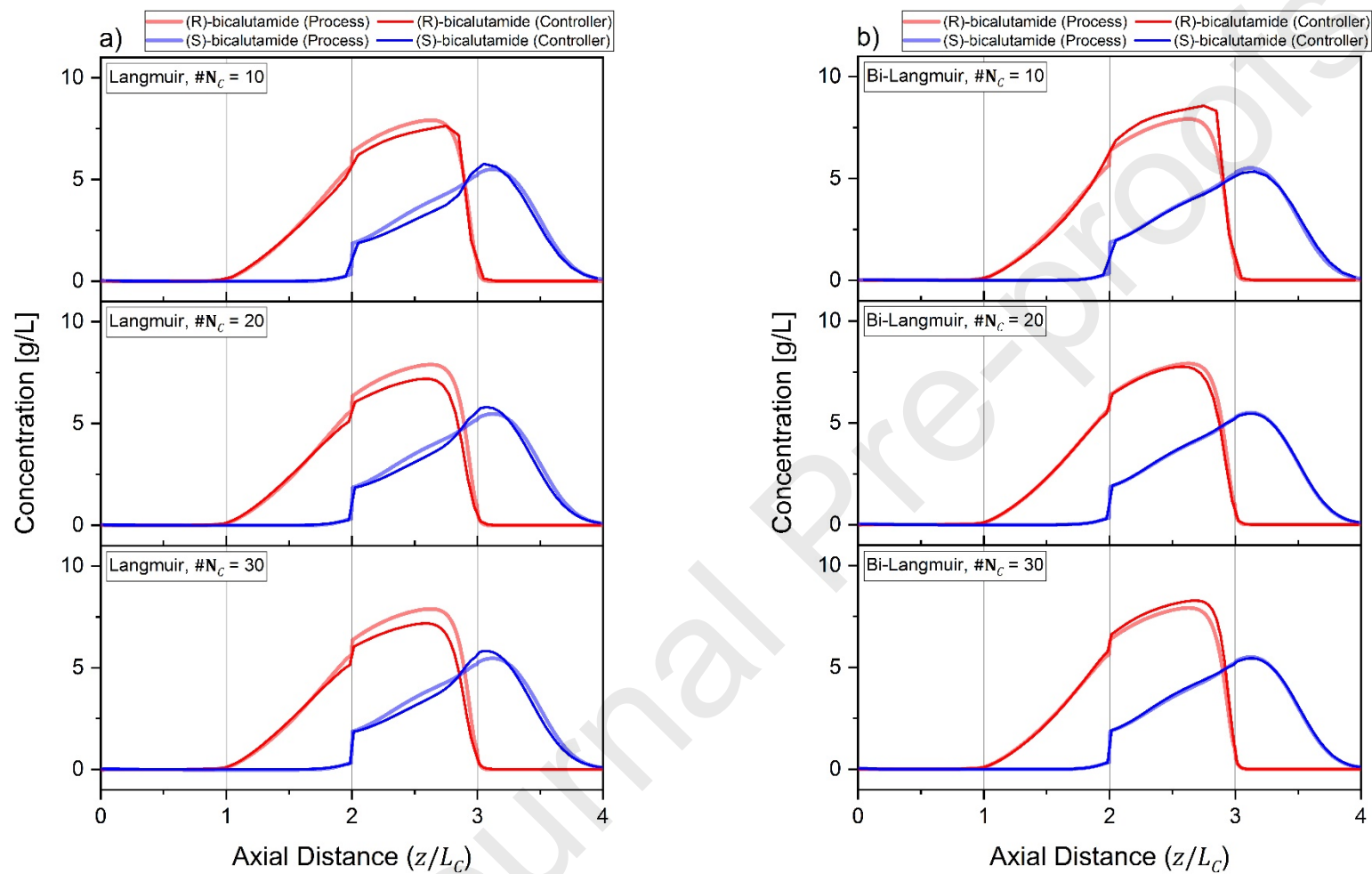


Figure 6.

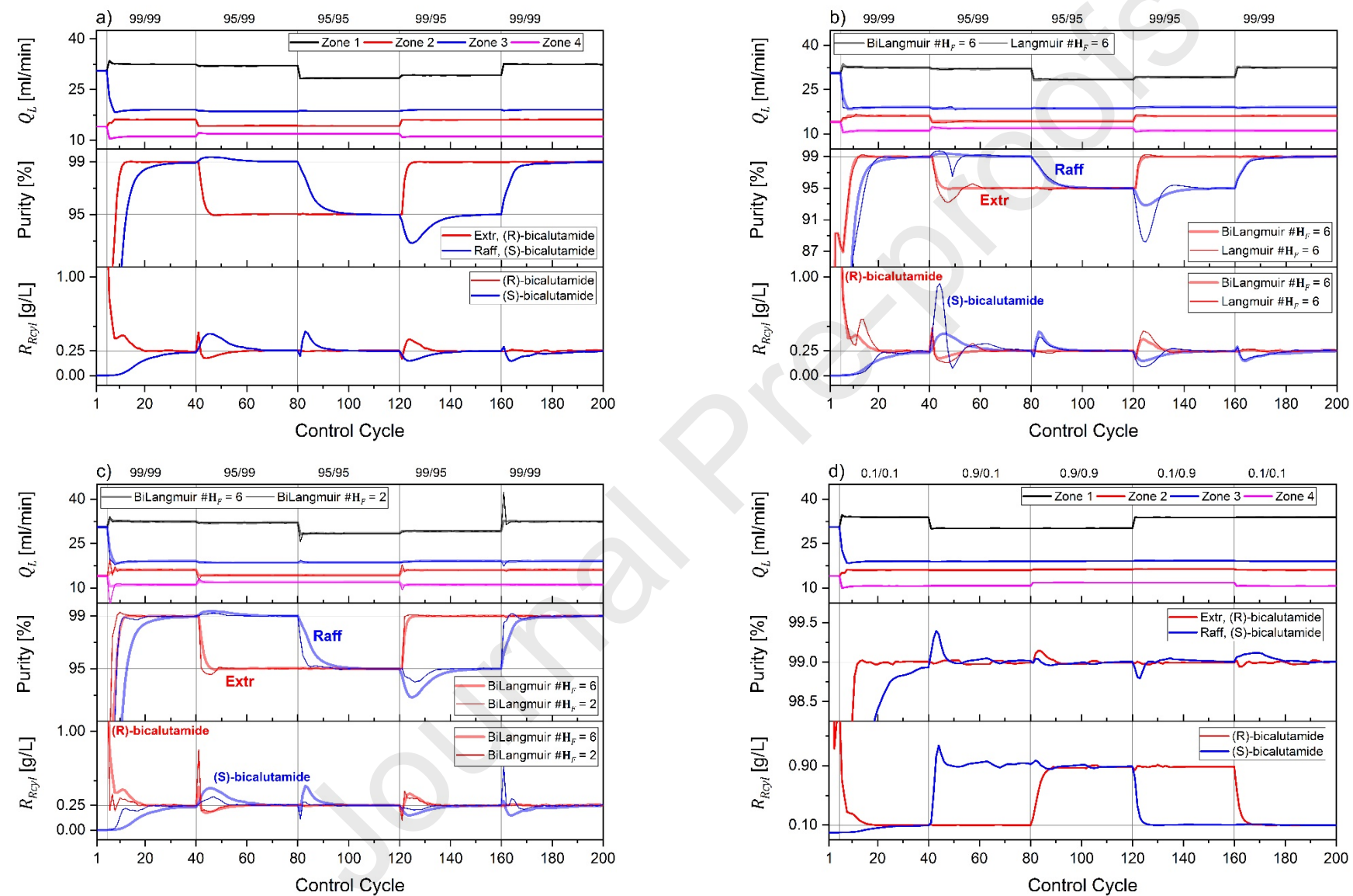


Figure 7.

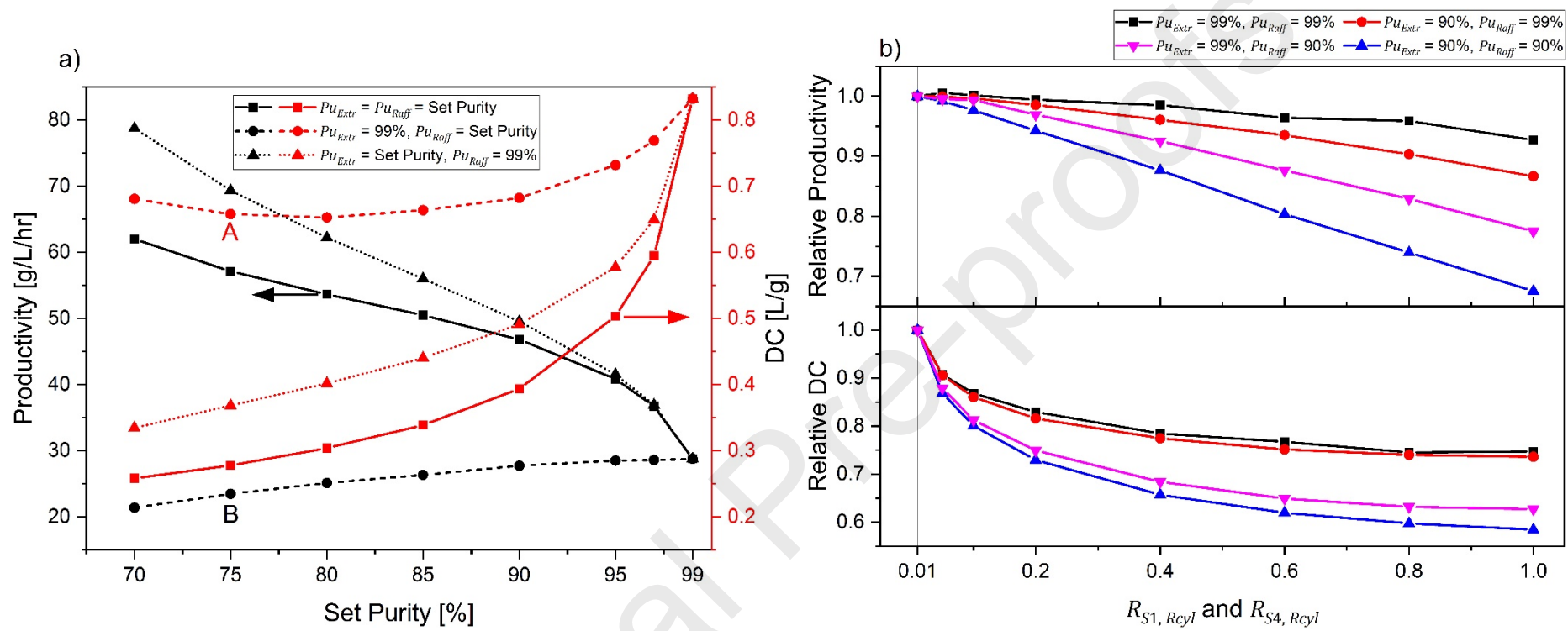


Figure 8.

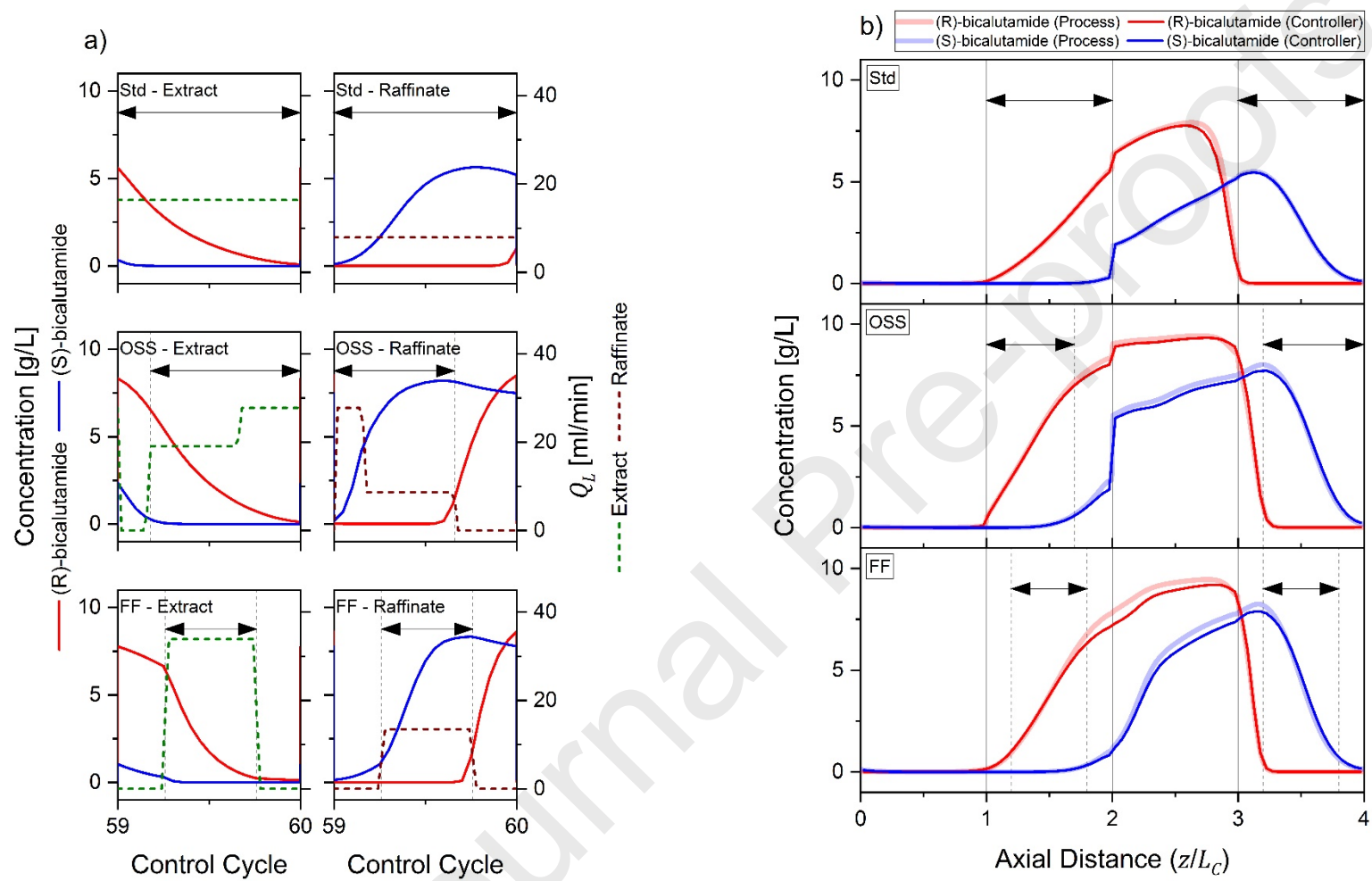


Figure 9.

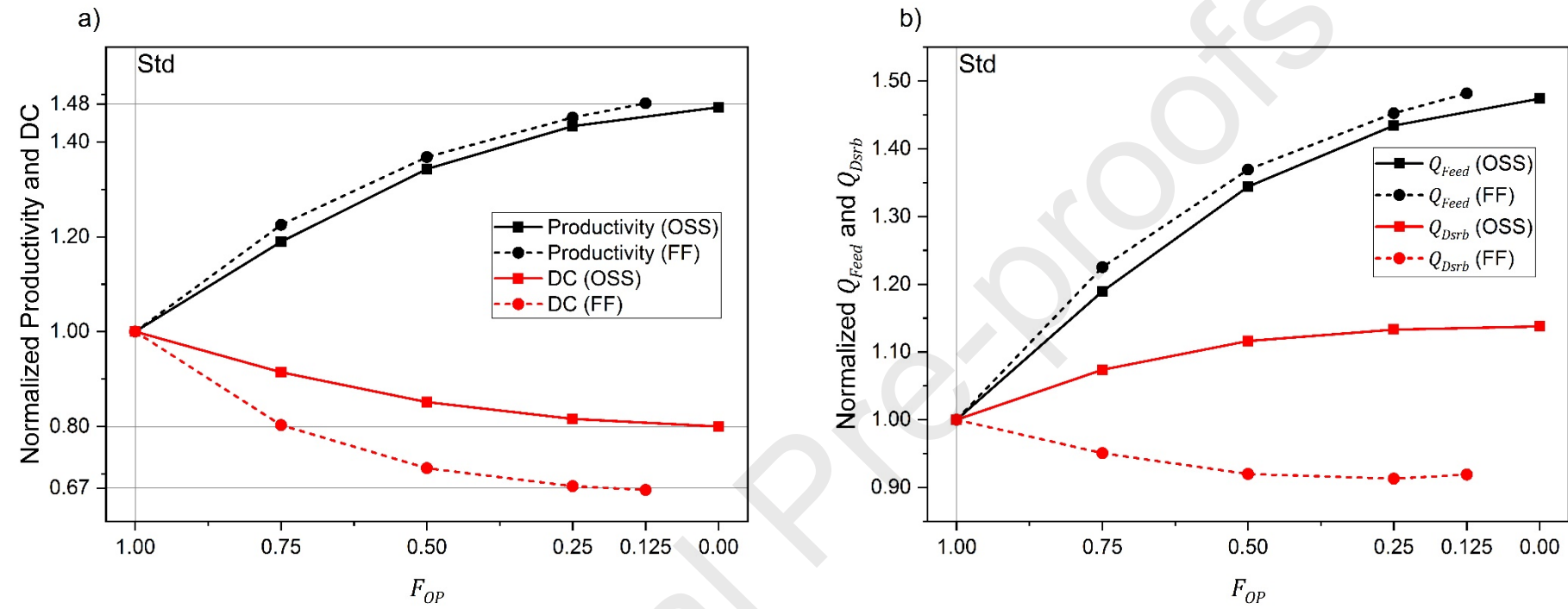


Figure 10.

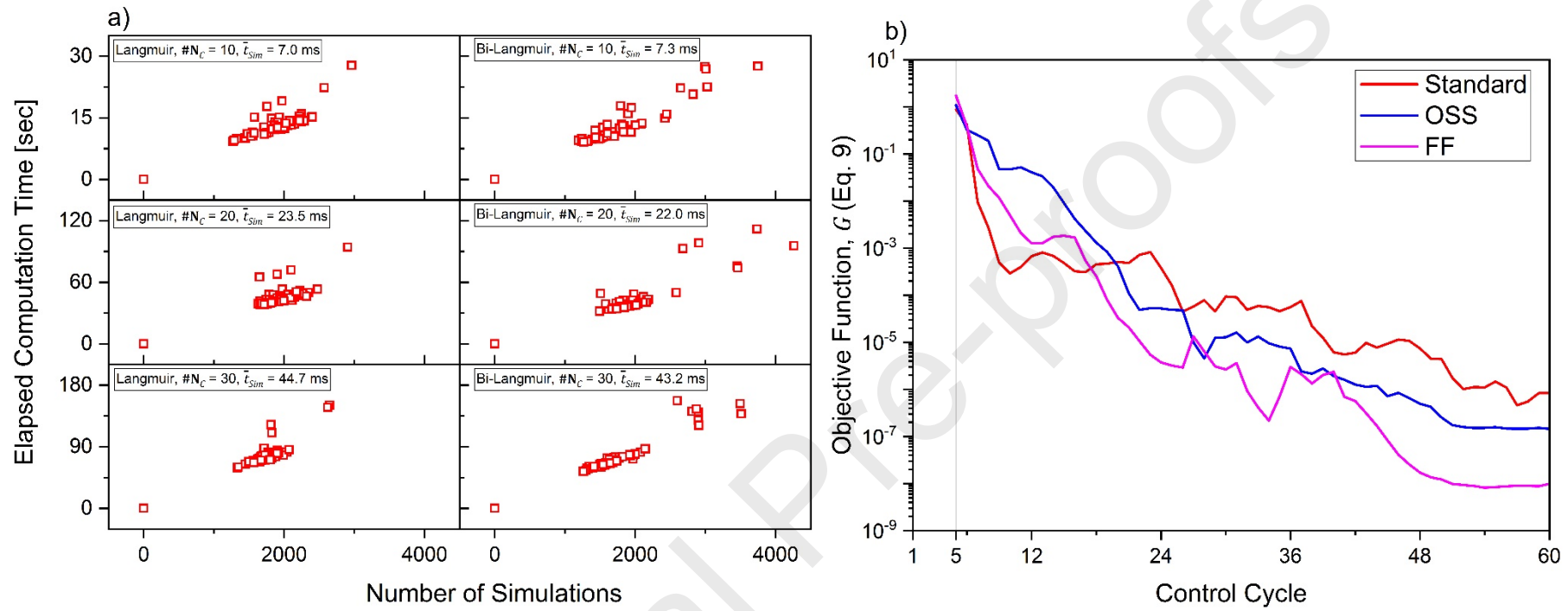
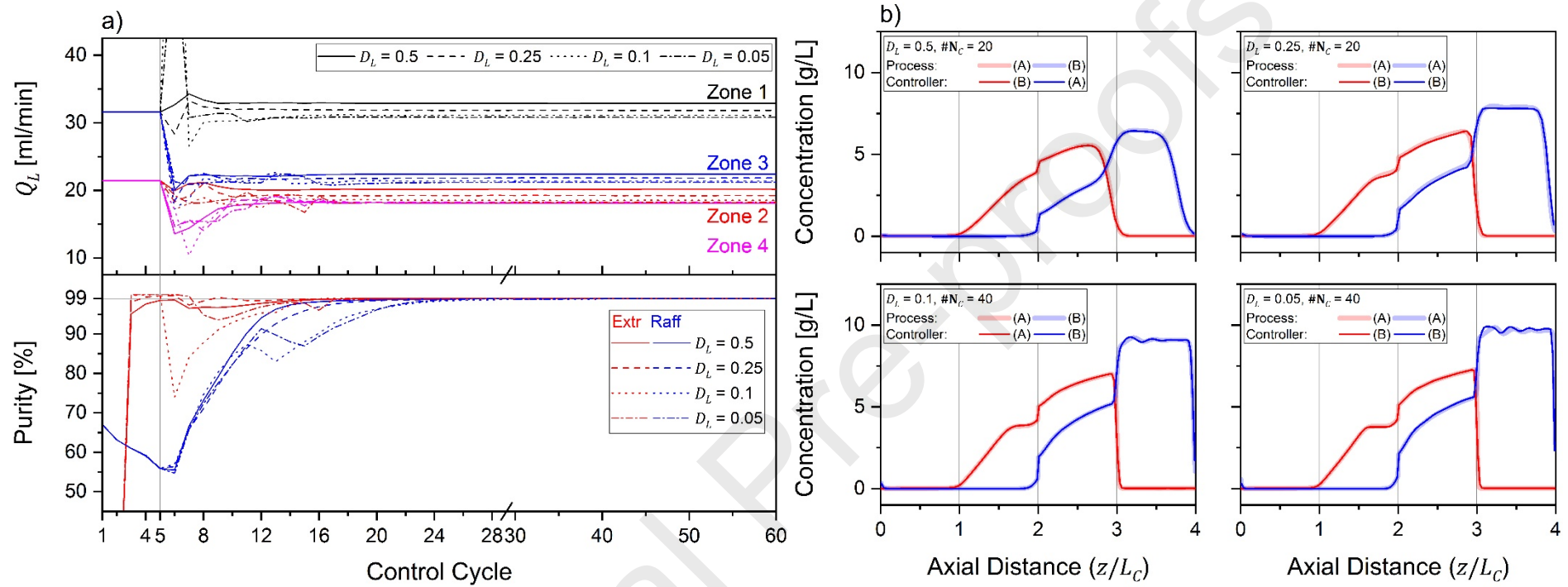


Figure 11.



## Credit Author Statement

Ju Weon Lee:

Conceptualization; Data curation; Formal analysis; Investigation; Methodology; Software; Validation; Visualization; Project administration; Roles/Writing - original draft; Writing - review & editing.

Achim Kienle:

Supervision; Roles/Writing - original draft; Writing - review & editing

Andreas Seidel-Morgenstern:

Supervision; Funding acquisition; Project administration; Resources; Roles/Writing - original draft; Writing - review & editing.

**Declaration of interests**

The authors declare that they have no known competing financial interests or personal relationships that could have appeared to influence the work reported in this paper.

The authors declare the following financial interests/personal relationships which may be considered as potential competing interests:

- On-line optimization of four-zone simulated moving bed processes using model based prediction of process states
- Fast and accurate estimation and prediction of process states by solving the equilibrium-dispersion model with the mixing cell with active counteraction scheme
- Successful theoretical validation of the proposed on-line optimization concept for the standard operating mode and two advanced operating modes